The Ising model on tetrahedron-like lattices: a finite-size analysis

1994 J. Phys. A: Math. Gen. 27 2965

(http://iopscience.iop.org/0305-4470/27/9/013)

J. Phys. A: Math. Gen. 27 (1994) 2965–2983. Printed in the UK

The Ising model on tetrahedron-like lattices: a finite-size analysis

O Diego†§, J González†‖ and J Salas‡¶

† Instituto de Estructura de la Materia, Serrano 123, 28006 Madrid, Spain

‡ Departamento de Física Teórica C-XI, Universidad Autónoma de Madrid, Cantoblanco, 28049 Madrid, Spain

Received 9 December 1993

Abstract. We study, using dimer and Monte Carlo approaches, the critical properties and finite-size effects of the Ising model on honeycomb lattices folded on the tetrahedron. We show that the main critical exponents are not affected by the presence of conical singularities. The finite-size scaling of the position of the maxima of the specific heat does not match, however, with the scaling of the correlation length, and the thermodynamic limit is attained faster on the spherical surface than in corresponding lattices on the torus.

1. Introduction

The Ising model conveys, in its simplicity, a richness of physical information which makes it relevant as a model for critical phenomena in different instances (ferromagnetic materials, lattice gas, binary alloys etc). The model is also paradigmatic of a common situation in statistical physics since, being one of the simplest models, it only allows analytic computation of the thermodynamic limit for particular classes of lattices (in one or two dimensions). In two dimensions, the Ising model in a square lattice has been solved in the continuum limit with cylindrical and toroidal boundary conditions [1, 2]. It has also been solved analytically for the two-dimensional model on a triangular or honeycomb lattice [3]. In general, however, the introduction of more specific boundary conditions precludes the resolution of the model in closed analytic form.

On the other hand, when resorting to a numerical simulation of the observables one may take advantage of finite-size effects to infer the critical behaviour in the thermodynamic limit [4]. However, finite-size effects depend, in general, on the boundary conditions in a way that may not be crucial but that cannot be predicted. There are several situations in which the asymptotic dependence on the spatial dimensions of the lattice has been rigorously studied. One of these cases corresponds to the analysis, by Ferdinand and Fisher, of the two-dimensional Ising model on large toroidal lattices [5]. The conclusions reached there support, in essence, the assumptions made in discussing finite-size effects and, more precisely, the hypothesis of finite-size scaling [6]. Some open questions are raised, however, regarding the approach to the critical coupling, which is drastically influenced by the shape of the torus.

§ e-mail: imtod67@cc.csic.es

‖ e-mail: imtjg64@cc.csic.es

¶ Present address: Physics Department, New York University, 4 Washington Place, New York, NY 10003, USA (e-mail: salas@mafalda.physics.nyu.edu).

0305-4470/94/092965+19$19.50

The purpose of the present paper is to investigate the finite-size effects and critical properties of the Ising model on a class of two-dimensional lattices with spherical topology. Our choice for the elements of this class is not arbitrary, but is rather dictated by a prescription which makes it possible to increase the size of the lattice without changing the local geometry. We propose to consider a type of honeycomb lattice folded on the tetrahedron, built from triangular blocks of the kind shown in figure 1 to form the faces of the polyhedron. One may construct a whole family of these lattices with increasing size, in such a way that the member of the Nth generation Δ_n has a number of lattice points equal to $n = 12N^2$. The coordination number is constant in each lattice. Moreover, from the point of view of the simplicial geometry, the curvature is always concentrated at the same faces, i.e. those formed by the three-fold rings around the four vertices. In principle, this clearly defines the problem of taking the thermodynamic limit along our sequence of lattices. In [7], clear evidence was given of critical behaviour in the ferromagnetic regime, as well as evidence supporting the hypothesis of finite-size scaling applied to the model on the curved surface.

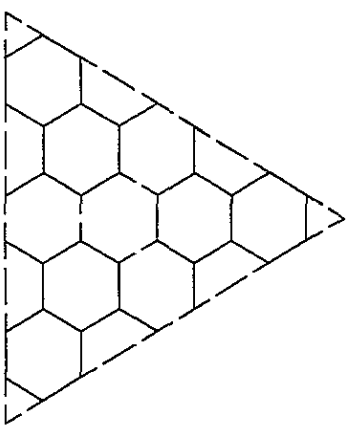

Figure 1. A generic triangular block for honeycomb lattices embedded on the tetrahedron.

The lattices we are considering may be understood by applying non-trivial boundary conditions for the honeycomb lattice on the plane, though they have the effect of introducing curvature into the model. We investigate the influence of these boundary conditions on finite-size effects and, more significantly from the physical point of view, on the critical properties of the model. Regarding the first point, we shall see that a discrepancy arises between the scaling of *pseudocritical* coupling constants for finite lattices and the true scaling of the correlation length. The second issue may probably be addressed in the continuum. In fact, the effect of boundary conditions in conformal field theories has been investigated before [8]. However, the inclusion of a conical singularity requires the kind of boundary condition which may call for a non-local operator in the theory [9], so the analysis of our model in the continuum does not appear to be so straightforward.

In this paper we apply two different numerical approaches: dimers and Monte Carlo (MC) simulations. The first one is very useful for small lattices (up to 1452 sites) and provides very accurate results for the specific heat and two-point correlators. However, this method cannot be used to extract information about the susceptibility of any finite system and for large lattices and, moreover, it demands a huge storage memory not available in

most computers. On the other hand, MC simulations are the standard tool for performing such computations at any lattice size, but the typical error bars of the measured quantities are much larger than those given by the former method. By combining both methods, we are able to provide better estimates and thus more reliable results.

The content of the paper is as follows. In section 2 we review the dimer approach applied to the computation of the partition functions and correlation functions of the model. Section 3 is devoted to the finite-size analysis of the data obtained with the above method, clarifying the issue concerning the ν critical exponent. In section 4 we give technical details of the MC simulations carried out to measure some of the larger lattices. Section 5 contains the results for the critical exponents α, β, γ obtained after combining data from the dimer approach and the MC simulations. Finally, we draw our conclusions and outline further directions for our work.

2. The dimer approach to the Ising model

We review in this section the dimer formulation of the two-dimensional Ising model [10, 11]. This approach presents the advantage of being applicable to lattices with an irregular coordination. It enables us to write partition functions and correlation functions in closed compact form, essentially in terms of the determinants of some coordination matrices for the lattice. This is something that cannot be achieved for our curved lattices by any other standard resolution method for the two-dimensional Ising model. There is no obvious way, for instance, as to how to apply the transfer-matrix method to write down the partition function for a lattice with the topology of the sphere, not even to produce a numerical computation of the same result. Within the dimer approach, one may, in principle, compute the partition function for any of the hexagonal lattices inscribed on the tetrahedron. Although we have not been able to infer from this construction the thermodynamic limit along the sequence of growing lattices, the method is very efficient in calculating observables like the specific heat or the correlation length, with arbitrary precision. One can easily progress to lattices with more than 1000 points, with the possibility of applying a finite-size analysis to study the critical behaviour of the model.

The dimer formulation of the Ising model first makes use of the equivalence between the partition function of the model and the dimer partition function of a certain decorated lattice built from the original one [2]. Afterward, one may apply powerful techniques developed to perform the sum over dimer configurations. Let us review the former correspondence for the hexagonal lattice while allowing for some kind of frustration which keeps the coordination number over the lattice constant. Given a collection of spins $\{\sigma_i\}$, with i running over all the lattice points, the partition function $\mathcal{Z}$ is defined as the sum over all possible configurations

$$\mathcal{Z} = \sum_{\sigma_i = \pm 1} \mathrm{e}^{-JH} \tag{1}$$

where the Hamiltonian H is given by the sum over all the lattice links $\langle i, j \rangle$

$$H = -\sum_{\langle i,j \rangle} \sigma_i \sigma_j. \tag{2}$$

The factor $1/kT$ is absorbed for simplicity in the definition of the nearest-neighbour coupling J. It is well known that (1) can be cast as a sum over all the closed loops over the lattice.

Calling this collection $\{l_i\}$ and $\{n_i\}$ the respective numbers of links in the paths, we have actually

$$Z = (\cosh J)^l \sum_{\{l_i\}} (\tanh J)^{n_i} \tag{3}$$

l being the total number of links of the lattice. One can draw a correspondence between each closed path and a dimer configuration in the appropriate decorated lattice. This is formed in our model by inserting a triangle in place of each of the points of the original lattice. To each of these one may assign four different states, depending on whether the point is traversed or not by a closed path and on the direction in the first instance. These states are labelled in figure 2. In a similar fashion, there are four different possible configurations for the dimers on each triangle and the adjacent links of the decorated lattice which bear a one-to-one correspondence with the above states. These dimer configurations are labelled in figure 3. One may easily be convinced that, by establishing the equivalence between the respective states in figures 2 and 3, a unique closed path can be reconstructed starting from a given dimer configuration in the decorated lattice, and *vice versa*. Furthermore, if a weight equal to $z = \tanh J$ is given to each dimer on a triangle link and this is equal to 1 for dimers joining neighbouring triangles, it is clear that the dimer partition function reproduces the sum in the Ising partition function (3).

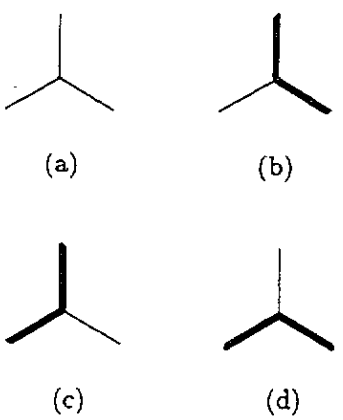

Figure 2. The different paths through a honeycomb lattice site.

There exist, in turn, powerful techniques developed for the computation of dimer partition functions, which rely mainly on the relation between these techniques and the Pfaffians of appropriate coordination matrices on the decorated lattice. We sketch here this relation, which has been worked out quite rigorously in [11]. The first step is to establish an order relation among the points of the decorated lattice. Once this is done, one may assign a matrix element $a_{p_1 p_2}$ for points numbered p_1 and p_2 such that $a_{p_1 p_2} = \tanh J$ if the points belong to the same triangle, $a_{p_1 p_2} = 1$ if they are nearest neighbours belonging to different triangles, and $a_{p_1 p_2} = 0$ otherwise. The sum over all dimer configurations, weighted as proposed before, is equivalent to performing the sum over all permutations $\{p_1, p_2, \ldots p_K\}$†

$$\sum a_{p_1 p_2} a_{p_3 p_4} \ldots a_{p_{K-1} p_K} \tag{4}$$

† K is the total number of points in the decorated lattice.

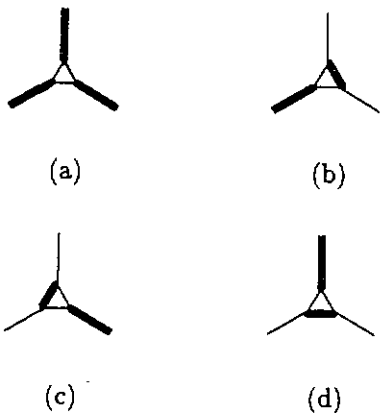

Figure 3. The dimer configurations around a triangle of the decorated lattice.

restricted by $p_1 < p_3 < \ldots p_{K-1}$ and $p_1 < p_2, p_3 < p_4, \ldots, p_{K-1} < p_K$. While there is no known algorithm to compute a sum of this kind efficiently, one may think of allowing for an antisymmetric matrix $A = \{a_{ij}\}$, so that the dimer partition function (a sum of all positive terms) may become proportional to

$$\sum (-1)^P a_{p_1 p_2} a_{p_3 p_4} \ldots a_{p_{K-1} p_K} \tag{5}$$

with $p_1 < p_3 < \ldots < p_{K-1}$ and $p_1 < p_2, p_3 < p_4, \ldots, p_{K-1} < p_K$, as before, and $(-1)^P$ being the signature of the permutation. Expression (5) reproduces the definition of the Pfaffian of the matrix A, which may be subsequently computed as the square root of its determinant. The remarkable conclusion which follows from the work of [2] is that, for planar lattices, it is always possible to choose the sign of the nearest-neighbour matrix elements $a_{p_1 p_2}$ so that all the terms in the sum (5) have the same sign. Since the matrix A becomes antisymmetric, it is customary to fix the sign of each $a_{p_1 p_2}$ pictorically by giving an orientation to every link of the decorated lattice—$a_{p_1 p_2}$ is positive, for instance, if the arrow goes from p_1 to p_2. We may enunciate the Kasteleyn theorem by saying that in any planar lattice there is always a system of arrows such that the dimer partition function can be computed as the Pfaffian of the corresponding antisymmetric coordination matrix.

The lattices we consider here fall into the category of planar lattices since they have the topology of the sphere. As long as we are interested in dimers mainly for computational purposes, we simply give the recipes which have to be followed to form the appropriate system of arrows on a planar lattice. Once superimposed on the plane, the lattice is made of so-called elementary polygons which are closed cycles that do not contain points in their interior. On the other hand, a polygon is said to be clockwise odd if the number of arrows pointing in the clockwise direction in the polygon is odd. The basic results which hold for planar lattices are (i) that it is always possible to choose a system of arrows such that all the elementary polygons are clockwise odd; and (ii) that with this choice and taking $a_{p_1 p_2}$ as positive when the arrow goes from p_1 to p_2, all the terms in the expansion of the Pfaffian (5) have the same sign.

In our case, a possible system of arrows realizing property (i) for a decorated lattice inscribed on the tetrahedron is shown in figure 4, where all the arrows for the triangle links (not drawn) are supposed to point in the clockwise direction. The advantage of this choice of arrows is that it keeps a regular pattern in the bulk, while only a few arrows on

the boundary links have to be flipped to make all elementary polygons clockwise odd. In general, progressing to the next member of our family of lattices on the tetrahedron just amounts to adding a column of (decorated) hexagons at each side of figure 4 and expanding the vertical dimension appropriately. The proposed system of arrows may be extended in a straightforward way to larger lattices. According to the above discussion, we always set the absolute value of the matrix elements $a_{p_1p_2}$ equal to $\tanh J$ for points in the same triangle and equal to 1 for nearest neighbours on different triangles. The partition function for any honeycomb lattice on the tetrahedron can be represented, therefore, in terms of the respective matrix A by

$$\mathcal{Z} = (\cosh J)^l (\det A)^{1/2}. \tag{6}$$

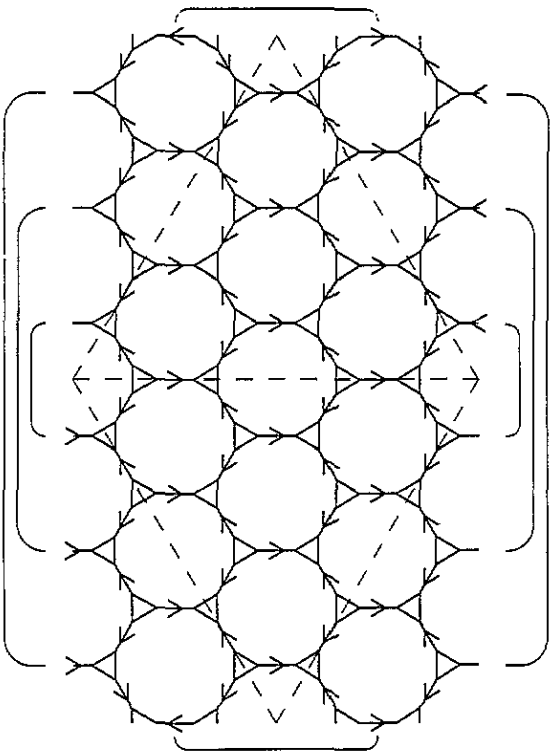

Figure 4. The decorated lattice for the second generation. The outer lines show the identifications of boundary links which embed the lattice onto the tetrahedron.

We have made use of representation (6) to perform the numerical computation of the maximum of the specific heat (in the ferromagnetic regime) for lattices up to Δ_{1452}. In practice, we have calculated the determinant using the subroutines of an IMSL Library implemented on a VAX 9000 machine. In this procedure, the lower triangular–upper triangular factorization of the matrix A is performed and the main limitation is the size of the available computer memory for the storage of huge number of matrix elements. The factorization of the matrix corresponding to Δ_{972}, for instance, is reached in less than 6 min of CPU time. Furthermore, the numerical computation of the derivatives of $\mathcal{Z}$ has

been carried out using subroutines from the NAG Library which rely on an extension of the Neville algorithm. With this method we have been able to measure this quantity with a relative error of less than 10^{-7} in most cases. Correspondingly, precise determination of the coupling constant, at which the maximum is attained in each lattice, has also been possible (see table 1). The values of these pseudocritical coupling constants are fundamental ingredients for the finite-size analysis to be accomplished in the next section. We have also computed the values of the specific heat of the curved lattices at the critical coupling constant of the planar honeycomb lattice (see table 2). These are also relevant under the hypothesis of finite-size scaling since, as we shall see, the sequence of pseudocritical temperatures converges in the thermodynamic limit to the critical temperature of the planar hexagonal lattice.

Table 1. For each lattice size N we show the values of the maximum of the specific heat and its positions ($CV_{\max}$, $J_N(CV)$) and the same values for the susceptibility ($\chi_{\max}$, $J_N(\chi)$). Those values marked with † were computed using the exact partition function [7], those with ‡ using the dimer approach (see section 2) and those with • by evaluating exactly (and numerically) the partition function. The rest were obtained by means of the MC simulations described in section 3.

N	$CV_{\max}$	$J_N(CV)$	$\chi_{\max}$	$J_N(\chi)$
1	1.439 235 51(1)†	0.467 332(1)‡	1.256 427 8(1)*	0.487 805(1)*
2	1.652 045 95(1)†	0.608 224(1)†		
3	1.892 382 32(1)†	0.634 238(1)†	7.91(2)	0.6215(3)
4	2.079 777 38(1)‡	0.643 862(1)‡		
5	2.230 815 51(1)‡	0.648 580(1)‡	18.98(7)	0.6377(3)
6	2.356 827 45(1)‡	0.651 275(1)‡		
7	2.464 773 96(1)‡	0.652 973(1)‡	34.4(1)	0.6444(2)
9	2.642 880 48(1)‡	0.654 929(1)‡	53.3(2)	0.6480(2)
11	2.786 536(6)‡	0.655 98(5)‡	75.9(4)	0.6498(2)
15	3.02(1)	0.6571(3)	128.4(8)	0.6523(2)
21	3.30(2)	0.6579(3)	232(2)	0.6540(2)

Table 2. For each lattice size N we show the values of the specific heat $CV_N(J_c)$, the susceptibility $\chi_N(J_c)$ and the magnetization $M_N(J_c)$ evaluated at the critical point J_c^{torus}. The symbols possess the same meaning as in table 1.

N	$CV_N(J_c)$	$\chi_N(J_c)$	$M_N(J_c)$
1	0.993 504 89(1)†	0.861 702 0(1)*	0.828 688 06(1)*
2	1.516 399 51(1)†		
3	1.817 465 16(1)†	6.889(3)	0.6904(9)
5	2.194 656 54(1)‡	16.89(9)	0.645(1)
6	2.328 986 39(1)‡		
7	2.442 490 02(1)‡	30.8(1)	0.6168(7)
9	2.627 440 12(1)‡	48.2(3)	0.597(1)
11	2.77(1)	68.3(4)	0.5828(9)
15	2.998(9)	116(1)	0.560(1)
21	3.24(1)	210(2)	0.536(2)

We conclude this section with an outline of how the two-point correlation functions can be obtained within the dimer approach [10, 11]. Given two arbitrary spins σ_p and σ_q in the

lattice, their average

$$\langle \sigma_p \sigma_q \rangle = \frac{1}{Z} \sum_{\sigma_i = \pm 1} \sigma_p \sigma_q \mathrm{e}^{-JH} \tag{7}$$

may be computed with the following trick. One chooses a path C from σ_p to σ_q on the lattice, which will comprise a number of consecutive spins $\{\sigma_{p_1}, \sigma_{p_2}, \ldots, \sigma_{p_m}\}$. The two-point function may also be expressed as

$$\langle \sigma_p \sigma_q \rangle = \frac{1}{Z} \sum_{\sigma_i = \pm 1} \sigma_p \sigma_{p_1} \sigma_{p_1} \ldots \sigma_{p_{m-1}} \sigma_{p_m} \sigma_q \mathrm{e}^{-JH}. \tag{8}$$

Now we have that $\sigma_p \sigma_{p_1}, \sigma_{p_1} \sigma_{p_2}, \ldots, \sigma_{p_m} \sigma_q$ are pairs of nearest-neighbour spins. Therefore, we find

$$\langle \sigma_p \sigma_q \rangle = \frac{1}{Z} \sum_{\sigma_i = \pm 1} \prod_{\langle i,j \rangle \notin C} (\cosh J + \sigma_i \sigma_j \sinh J) \prod_{\langle k,l \rangle \in C} (\sinh J + \sigma_k \sigma_l \cosh J) \tag{9}$$

where the first product extends to all the links which do not belong to C and the second product runs over the links that do belong to the path. From (9), we arrive finally at the expression

$$\langle \sigma_p \sigma_q \rangle = \frac{1}{Z} (\cosh J)^l (\tanh J)^{m+1} \sum_{\{l_i\}} (\tanh J)^{n_i - r_i} \frac{1}{(\tanh J)^{r_i}} \tag{10}$$

where the sum, as in expression (3), is over all the closed loops on the lattice but with the difference that the number r_i of links in each loop belonging to C now have to be weighted with $(\tanh J)^{-1}$ rather than with $\tanh J$. It becomes obvious that all the machinery of the dimer formulation can be applied again to transform the sum in (10) into a suitable dimer partition function on the decorated lattice, so that

$$\langle \sigma_p \sigma_q \rangle = \frac{1}{Z} (\cosh J)^l (\tanh J)^{m+1} (\det A')^{1/2}. \tag{11}$$

The appropriate coordination matrix $A' = \{a'_{ij}\}$ has to keep track of the different weights that the $m + 1$ links in C carry in the sum over the closed loops.

3. Finite-size scaling and critical exponents

3.1. Finite-size scaling

It is well known that singularities in the free energy (i.e. phase transitions) can only occur in the thermodynamic limit. For finite volumes the free energy is an analytic function of the temperature and any other parameter in the Hamiltonian. The thermodynamic singularities are thus smoothed out around the transition point. A trace of the existence of such non-analyticities is the presence of some peaks in the specific heat CV or magnetic susceptibility χ curves. The dependence of the linear size of the system L on the location of the maxima of these peaks and their height enables the thermodynamic limit to be described from finite-size data [4].

In second-order phase transitions this round-off is due to the fact that the correlation length ξ is limited by the size of the system. This fact defines a pseudocritical coupling $J^*(L)$ such that

$$\xi(J^*(L)) \sim L. \tag{12}$$

At this point the surface contribution to the free energy is not negligible compared to the bulk energy. In the vicinity of a second-order transition point J_c, the correlation length diverges with a power-law given by

$$\xi(J) \sim (J - J_c)^{-\nu}. \tag{13}$$

From (12) and (13) the dependence of the pseudocritical coupling on the lattice size can be derived:

$$|J^*(L) - J_c| \sim L^{-1/\nu}. \tag{14}$$

Unfortunately in practical situations it is a very involved task to compute such a quantity $J^*(L)$. It is easier to look at the position and height of the peaks mentioned above. If some quantity P diverges near the critical point† as

$$P(J) \sim |J - J_c|^{-\rho} \qquad \rho > 0 \tag{15}$$

then it can be shown [4] that for a finite volume it attains a maximum value $P_{max}(J_L)$ at a point $J_L(P)$ given by

$$|J_L(P) - J_c| \sim L^{-\theta_P} \tag{16a}$$

$$P_{max}(J_L) \sim L^{\rho/\nu} \tag{16b}$$

when L is large enough. In most systems it is found that

$$\theta_P = \frac{1}{\nu} \tag{17}$$

but this is not a general result. There are some examples where this property does not hold: the spherical model, the ideal Bose gas [12] and the one-dimensional $q = \infty$ clock model [13]. In the present paper, we will face another situation in which the relation (17) is violated. On the other hand, if $\theta \geqslant 1/\nu$ then the behaviour of this quantity at finite volume evaluated at the critical point $P_L(J_c)$ is the same as in (16*b*)

$$P_L(J_c) \sim L^{\rho/\nu}. \tag{18}$$

Using (16*a*) and (16*b*) the critical coupling J_c and the critical-exponents ratio ρ/ν can be derived from finite-size data. When J_c is explicitly known and $\theta_P \geqslant 1/\nu$, then (18) can be used instead of (16*b*). In this paper we are mainly concerned with the analysis of the susceptibility and the specific heat. So, we will obtain estimates of J_c and the ratios γ/ν and α/ν. The rest of the critical exponents may be derived using the scaling relations [14]. In particular, in this paper we will check numerically the following equations:

$$\frac{\beta}{\nu} = 1 - \frac{\gamma}{2\nu} \tag{19a}$$

$$\frac{1}{\nu} = 1 + \frac{\alpha}{2\nu}. \tag{19b}$$

Independent estimates of ν and β/ν will be obtained in terms of the analysis of the correlation length (see below) and the magnetization at the critical point, respectively (see section 5).

† Hereafter, we will denote quantities computed in a finite volume with a subscript L meaning the linear size of the system (i.e. P_L). Whenever no subscript is present, the thermodynamic limit is assumed (i.e. $P = \lim_{L\to\infty} P_L$).

3.2. Critical point and exponent θ_{CV}

In section 2 we showed that for lattices up to Δ_{1452} we were able to obtain very accurate estimates of the internal energy E and the specific heat. These quantities are defined hereafter as follows:

$$E_N = \frac{2}{3V}\langle H \rangle \tag{20}$$

$$CV_N = \frac{3V}{2}\sigma^2\left(\frac{2}{3V}H\right) \tag{21}$$

where the factor $3V/2$ is equal to the number of links in a lattice of V sites and $\sigma(\cdot)$ is the standard deviation. Thus, the values of $CV_{\max}$ and $J_L(CV)$ can be computed with high precision. In what follows we will identify the lattice linear size L with the index N characterizing the fullerene lattice (see section 1). This choice is consistent as the volume increases as $V = 12N^2$.

Data will be fitted according to the power-law function $J_N(CV) = J_c + AN^{-\theta_{CV}}$ using a least-χ^2 method. Here the input errors are given by the precision of the computer in calculating $J_N(CV_{\max})$. In order to obtain a more reliable result, we will sequentially remove the point with smallest N. One can eventually observe a monotonic trend to some value, which will be identified with the thermodynamic limit.

Our best result is

$$J_c = 0.65\,850 \pm 0.00\,002 \tag{22}$$

for $5 \leqslant N \leqslant 11$. In this case $\chi^2 = 0.07$ with degrees of freedom. Throughout this paper all the errors associated with our final results will be equal to two standard deviations—i.e. 95% confidence level. The latter result is compatible with the critical point of the Ising model on a toroidal honeycomb lattice, $J_c^{\text{torus}} = \frac{1}{2}\log(2+\sqrt{3}) = 0.65\,848$, which can be derived easily using duality [14, 15]. Thus, our data strongly support the hypothesis that both critical points coincide.

A good estimate of θ_{CV} is obtained by repeating the fit with $J_c = J_c^{\text{torus}}$. The result is

$$\theta_{CV} = 1.745 \pm 0.015 \tag{23}$$

for $6 \leqslant N \leqslant 11$ and with $\chi^2 = 1.2$. This is in clear disagreement with the result expected for a lattice on a torus ($\theta_{CV} = 1$ [5]). This fact makes it necessary to determine the ν critical exponent, in order to see if the above measurement bears any relation to it (see below).

We will skip here the analysis of $CV_{\max}$ as there is a subtle difference between the logarithmic and power-law behaviours, particularly when such a power is rather small. This will be carried out in section 5.

3.3. Correlation length and exponent ν

An independent way to compute the critical exponent ν is to study the correlation length near the critical point. This quantity is defined in terms of the connected two-point function

$$\langle \sigma_0 \cdot \sigma_r \rangle^c = \langle \sigma_0 \cdot \sigma_r \rangle - \langle \sigma_0 \rangle \langle \sigma_r \rangle \sim e^{-r/\xi} \tag{24}$$

when r is large enough. The connected two-point correlators are equal to the usual ones $\langle \sigma_0 \cdot \sigma_r \rangle$ for $J < J_c$ (unbroken phase). This feature allows their exact computation

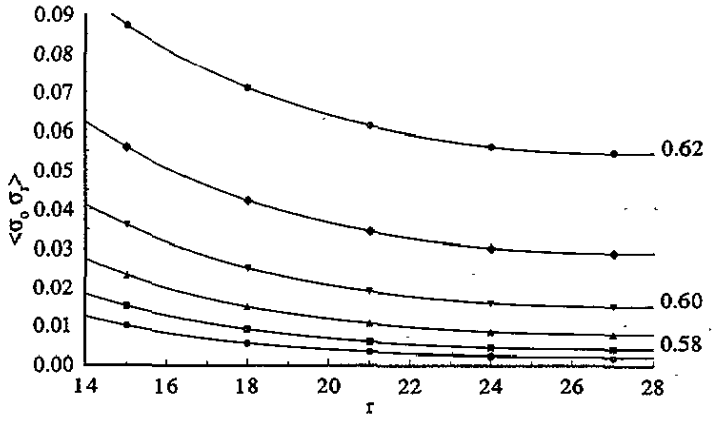

Figure 5. Values of the unsubstracted two-point correlators $\langle\sigma_r\sigma_0\rangle$ for different separations r and couplings constants $J = 0.57, 0.58, \ldots, 0.62$. The least-$\chi^2$ fits are also depicted.

using the machinery developed in section 2. (For finite lattices odd quantities such as the magnetization are always equal to zero, even in the broken phase.)

A major problem is how to recover $\xi_N(J)$ from the finite-volume correlators $\langle\sigma_0 \cdot \sigma_r\rangle_N$. For a torus of linear size L these functions are expected to behave as $\sim \cosh((x - L/2)/\xi_L)$ when $x \gg 1$. But this question is not clear for the truncated tetrahedron. On the other hand, it is well known [11] that the correlation length does depend on the direction in which the spins σ_r are disposed. However, the same critical behaviour is expected for all the possible directions.

This study has been carried out on the lattice Δ_{972}, which is the largest one allowed by our computer facilities. We believe that this one is large enough to see the thermodynamic limit. We have chosen couples of spins along the diagonal in the representation in figure 4 of the tetrahedron unfolded on the plane. Our choice for σ_r allowed us to introduce an increasing distance between spins running from $3, 6, \ldots$ up to 27 (in units of the lattice spacing). At $r = 27$, both spins are located at antipodal points. If we continue along the diagonal we finally arrive at σ_0. For this reason, we expect that the correlators will behave, for large r, like a symmetrized version of equation (24). In order to improve our results, we include in our ansatz the correct leading term for the square lattice on the torus [11]

$$\langle\sigma_0\sigma_r\rangle = \frac{f}{\sqrt{r}}e^{-r/\xi}(1 + \mathcal{O}(1/r)) \tag{25}$$

suitably symmetrized around $r = 27$.

We have analysed the cases $J = 0.58$, 0.59, 0.60, 0.61 and 0.62 (see figure 5). We have obtained extremely good fits for all these cases, giving differences of order $\sim 10^{-5}$. Although the lattice Δ_{972}, like any of the lattices inscribed on the tetrahedron, is not homogeneous, it is remarkable that the values of the two-point functions at each different J fit, to a high degree of precision, the correct leading behaviour for the Ising model on a square lattice on the torus. The deviation that we have found from the dependence (25) appears to be even smaller than for similar measurements carried out for the lattice on a torus. The estimated values of the correlation length are shown in figure 6 and will be used in the computation of the ν critical exponent. We tried unsuccessfully to fit data for $J > 0.62$ to (25). The reason is that very close to the critical point we have to take into account the $\mathcal{O}(1/r)$ (or even higher) terms in equation (25).

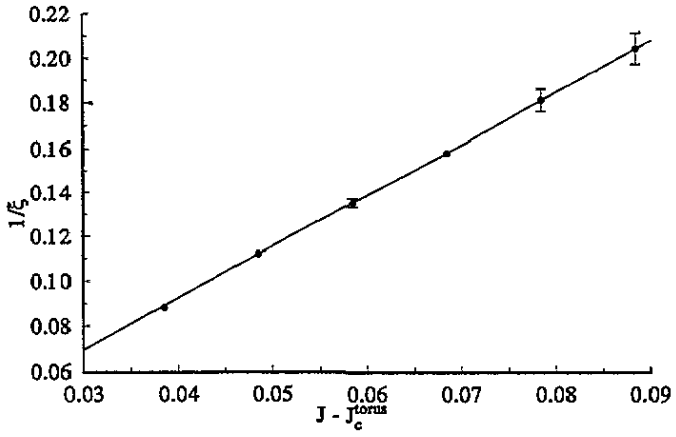

Figure 6. Values of $\xi(J)^{-1}$ for those J shown in figure 5. The straight line corresponds to the χ^2 fit.

We tried to fit the values of $\xi_{N=9}^{-1}(J)$ according to (13). We obtained a value equal to $\nu = 1.01 \pm 0.04$ with $\chi^2 = 0.36$. However, if we drop the point with $J = 0.62$ (the closest to J_c) the result is

$$\nu = 1.00 \pm 0.06 \tag{26}$$

with a remarkable small value for $\chi^2 \sim 7 \times 10^{-5}$.

The conclusions of the analysis of the data coming from the dimer computations can be summarized in the following points:

(a) the critical point is compatible with J_c^{torus};

(b) the critical exponent $\nu = 1.00 \pm 0.06$;

(c) the finite-size exponent $\theta_{CV} = 1.745 \pm 0.015$ is significantly different from $1/\nu$.

In summary, our results suggest that the critical properties of the Ising model on the truncated tetrahedron are the same as on the torus. However, we find a very clear difference in the finite-size behaviour of these models as long as the scaling of pseudocritical coupling constants (determined from the maxima of the specific heat) does not match the scaling behaviour of the correlation length. The thermodynamic limit is achieved much faster on the tetrahedron than on the torus, at least with regard to the specific heat.

4. Technical aspects of the MC simulations

We have performed several MC runs for different lattice volumes $V = 12N^2$ and coupling constants J. The relevant information about the simulations can be found in table 3.

We used a Metropolis algorithm with the R250 pseudo-random-number generator [16] initialized with the RANMAR subroutine. The period of such a generator is equal to $2^{250} - 1$. Recently, it has been claimed [16] that the combination of the Metropolis algorithm with the R250 generator gives better results than other more involved procedures. We have compared the values obtained by both the dimer approach and the direct MC simulation. They were consistent, within statistical error.

Table 3. Number of Monte Carlo steps performed for each simulation in a lattice of volume $V = 12N^2$ and coupling constant J.

N	J	MC steps
3	J_c^{torus}	3×10^6
3	0.62	3×10^6
5	J_c^{torus}	3×10^6
5	0.64	3×10^6
7	J_c^{torus}	12×10^6
9	J_c^{torus}	12×10^6
11	J_c^{torus}	12×10^6
15	J_c^{torus}	11×10^6
21	J_c^{torus}	12×10^6

In all cases, we have measured the internal energy density and the magnetization defined as

$$M_N = \left\langle \left| \frac{1}{V} \sum_i \sigma_i \right| \right\rangle. \tag{27}$$

We have also measured the specific heat and the magnetic pure-phase susceptibility

$$\chi_N = V\sigma^2 \left(\left| \frac{1}{V} \sum_i \sigma_i \right| \right). \tag{28}$$

In all cases, we discarded the first 10^5 MC steps for terminalization. Then we have measured each observable once every 100 MC steps. In this way we obtained statistically independent data, as they could be checked by computing the corresponding autocorrelation times [17].

In order to calculate the maximum value of the specific heat and the susceptibility we have used the spectral density method (SDM) [18]. At a given coupling J, we can obtain the histograms $N(E, M; J)$ which keep track of the numbers of configurations with magnetization M and internal density energy E. This information is enough to compute the expectation value of any function $f(M, E)$ at any other coupling J'. In our case, the magnetic field is zero and in equations (20), (21), (27) and (28) the observables do not depend on E and M simultaneously. For these reasons we could use the following formulae:

$$\langle f(E) \rangle (J') = \frac{\sum_E f(E) N_0(E; J) \exp\{(J' - J)E\}}{\sum_E N_0(E; J) \exp\{(J' - J)E\}} \tag{29}$$

$$\langle f(M) \rangle (J') = \frac{\sum_E N_f(E; J) \exp\{(J' - J)E\}}{\sum_E N_0(E; J) \exp\{(J' - J)E\}} \tag{30}$$

where the one-dimensional histograms are defined as follows

$$N_0(E; J) = \sum_M N(E, M; J) \tag{31}$$

$$N_f(E; J) = \sum_M f(M) N(E, M; J). \tag{32}$$

The SDM gives the correct answer for couplings J' close to the coupling J where the simulation was performed. A criterion for the applicability of such method is [18]

$$|J' - J| \sim \frac{1}{\sigma(E)V}. \tag{33}$$

In most cases, one simulation only at $J = J_c$ is enough to determine the maximum of CV and χ. However, for the smaller lattices an additional run had to be performed in order to obtain a reliable estimate of such quantities.

We have divided the entire sample into typically 30–120 subsamples, each containing $\sim$ 1000 measures. For each subsample we computed every quantity (including $CV_{\max}$, $J_N(CV), \ldots$). With these estimates we calculated the statistical errors using the jack-knife method [19]. In this way, the effect of correlation among data was taken into account.

We performed all the MC simulations on a VAX 9000 machine with a vectorial processor. The program was not fully vectorizable as the lattice could not be split into two disjoint sublattices, i.e. every element of one sublattice is surrounded by elements belonging to the other one†. However, we could divide the whole lattice into three subsets. The elements of the first two were arranged on two disjoint triangular sublattices, so that their update could be fully vectorized. On the other hand, the rest of the spins can be located on two lines joining pairs of vertices on the tetrahedron and their numbers depend explicitly on the planar representation of the lattice. For these, the update is clearly not vectorizable. However, their effect on the CPU time is not very important for the larger lattices, as their number behaves as $\sim V^{1/2}$.

5. Results of the MC simulations

5.1. Position of the critical point

Here we will repeat the analysis of section 3 but with all the data of table 1. For data from the dimer analysis, the input error will be taken as the precision of the subroutines used. For those from the MC simulations the error is given by the jack-knife method described in section 4. The data for $N > 11$ possess large error bars compared with others with smaller N. For this reason the fits presented in section 3 cannot have large variations. In fact, the final results are the same as those presented in the preceding section (equations (22) and (23)) and with similar χ^2 values (see figure 7).

If we repeat the same procedure with the susceptibility we obtain an estimate for J_c compatible with the later one, but with a larger error bar. If we fix this quantity to J_c^{torus} we arrive at the following estimate for the exponent θ_χ

$$\theta_\chi = 1.01 \pm 0.02 \tag{34}$$

for $9 \leqslant N \leqslant 21$ and $\chi^2 = 0.8$ (see figure 7).

We observe that θ_χ is close the value $1/\nu = 1$ to in agreement with the Ising model on the torus. We conclude that

$$\frac{1}{\nu} = \theta_\chi < \theta_{CV} \tag{35}$$

† This feature has to do with the onset of frustration in the antiferromagnetic regime.

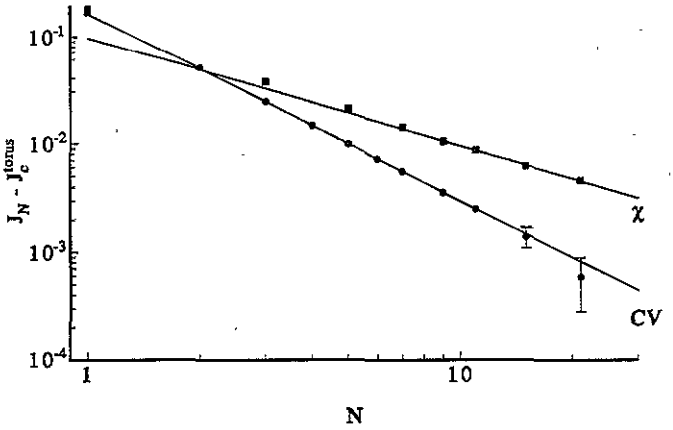

Figure 7. Values of the position of the maxima of the specific heat (circles) and the magnetic susceptibility (squares) with respect to the critical coupling J_c^{torus}. The power-law fits are also depicted.

and this feature implies that one can obtain the critical exponents using either equation (16*b*) or equation (18). As we have identified the critical coupling of our system, it seems more natural to rely on our conclusions on equation (18). In any case, the values obtained from equation (16*b*) are always consistent with those presented in this paper within statistical errors.

5.2. *Exponent ratios γ/ν and β/ν*

The value of γ/ν can be derived using the value of the critical magnetic susceptibility $\chi_N(J_c)$. We have fitted our data to $\chi_N(J_c) = AN^{\gamma/\nu}$ and our best result is $\gamma/\nu = 1.73 \pm 0.02$ for values of N ranging from 9 to 21 and with $\chi^2 = 0.79$. This is very close to the standard Ising model result $\gamma/\nu = 7/4 = 1.75$. If we fix γ/ν to this value we obtain a χ^2 value of ~ 2.8, which shows that the fit is reasonably good (see figure 8).

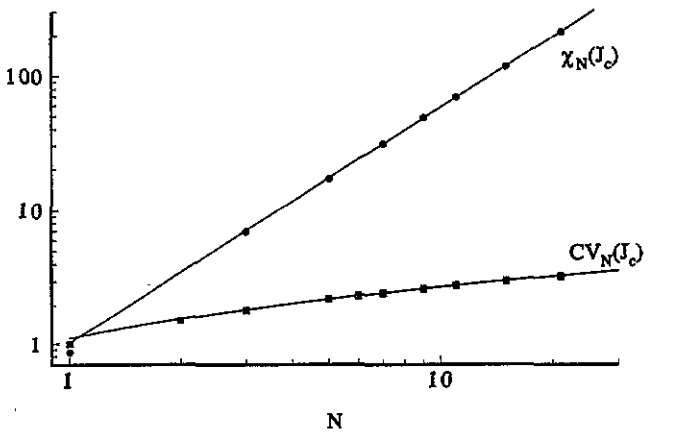

Figure 8. Power-law fits of the values of the specific heat (squares) and the magnetic susceptibility (circles) at the critical point J_c.

To determine the value of β/ν in an independent way (i.e. not using scaling relation (19*a*)) we will fix our attention on the magnetization at the critical point. In the thermodynamic limit, the magnetization near J_c behaves as

$$M(J) \sim |J - J_c|^{\beta}. \tag{36}$$

Using argument similar to those in section 3 it can be predicted that

$$M_N(J_c) \sim N^{-\beta/\nu}. \tag{37}$$

The result of performing such a fit is $\beta/\nu = 0.126 \pm 0.004$ using data with $7 \leqslant N \leqslant 21$ and with $\chi^2 = 0.33$ (see figure 9). This is also very close to the Ising value $\beta/\nu = 1/8 = 0.125$. This result supports the hypothesis that the scaling relation (19*a*) holds for this model.

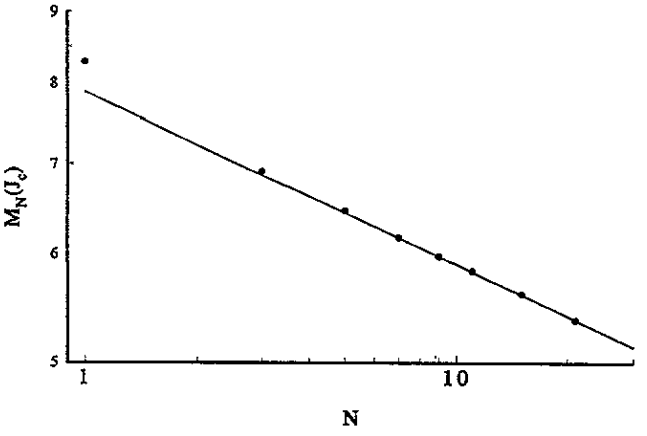

Figure 9. The same as in figure 8 for the magnetization $M_N(J_c)$.

This feature can be used in order to obtain a more accurate estimate of these exponents. We can try to fit $\chi_N(J_c)$ and $M_N(J_c)$ simultaneously using explicitly the relation (19*a*). The result is

$$\gamma/\nu = 1.748 \pm 0.008 \qquad \beta/\nu = 0.126 \pm 0.004 \tag{38}$$

Thus, our results strongly suggest that the ratio $\gamma/\nu = 7/4$, as in the Ising model on a torus. Notice that the error in this ratio is less than 0.6%.

5.3. Exponent ratio α/ν

We can perform the same routine for the specific heat and try to obtain the exponent ratio α/ν. If we try to fit data to a power-law function $CV_N(J_c) = A + BN^{\alpha/\nu}$, we do not obtain a satisfactory result. The best result gives a ratio $\alpha/\nu \sim 0.060$ with $\chi^2 \sim 9$ and $9 \leqslant N \leqslant 21$ (see figure 8). On the other hand, and motivated in part by the preceding results, we could try to fit the data to a logarithmic function. $CV_N(J_c) = A + B \log N$. In this case, the fit is successful giving a $\chi^2 = 1.9$ with $7 \leqslant N \leqslant 21$ (see figure 10). This immediately implies that

$$\alpha = 0 \tag{39}$$

and using equation (19*b*)

$$\nu = 1 \tag{40}$$

which is in agreement with the result from direct measurements of the correlation length displayed in section 3. Thus, both exponents take the same values as in the Ising model on the torus. On the other hand, we have also verified that the scaling relation (19*b*) does hold in this model.

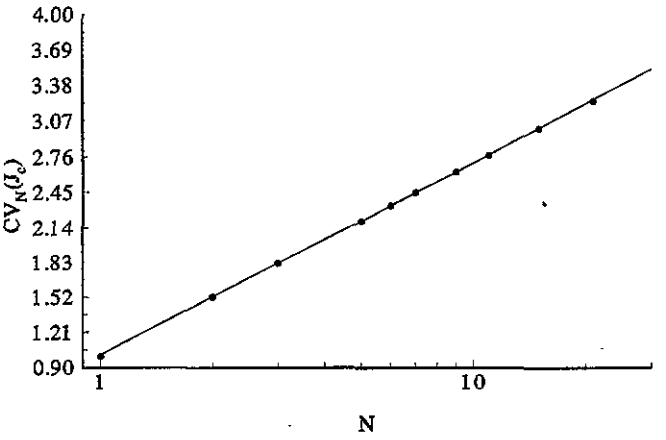

Figure 10. Logarithmic least-χ^2 fit of $CV_N(J_c)$.

6. Conclusions and outlook

In this paper we have presented the first fundamental study of the critical properties of an Ising model on a lattice with the topology of the sphere. In particular, we have chosen the family of honeycomb lattices that can be constructed on a tetrahedron. Our results can be summarized as follows.

(i) The dimer approach is very useful and competitive for lattices up to $\sim 10^3$ points. It provides very accurate data for the internal energy, specific heat and two-point correlators.

(ii) The critical properties of the Ising model on the tetrahedron are just the same as on the torus. In particular, we have checked that J_c is the same, as well as the critical exponents ν, α, γ and β.

(iii) We have also checked the validity of two scaling relations (19*a*) and (19*b*) among these exponents.

(iv) The finite-size scaling properties of these two systems are not the same. In our case, the position of the maxima of the specific heat scales near J_c with a critical exponent that does not bear any relation to the critical behaviour of the correlation length. That is, the thermodynamic limit is achieved faster on the tetrahedron. However, the behaviour of the susceptibility is the same in both cases.

Our results suggest that the same analysis carried out for other types of lattice with the same topology will yield the same conclusions: the critical behaviour will not change,

although variations in their finite-size properties would be expected to hold. All of them would belong to the same universality class of the Ising model on a torus.

On the other hand, the Ising model on the tetrahedron can be viewed as the Ising model with some non-standard boundary conditions. These non-standard conditions have the advantage that the critical behaviour is reached faster than for periodic boundary conditions.

Ferdinand and Fisher [4, 5] studied how the exponent θ_{CV} varies for the Ising model defined on a square lattice on an $m \times n$ torus. They concluded that $J_l(CV)$ behaves as

$$\frac{J_l(CV)}{J_c^{\text{torus}}} = 1 + \frac{b(\eta)}{l} + o(l^{-1}) \tag{41}$$

where $l = (m^{-2} + n^{-2})^{-1}$ measures the linear size of the torus and $\eta = m/n$ is its shape. They also showed that $b(\eta)$ is not a monotonic function of η. In particular, $b(\eta) > 0$ in the range $\eta \in (\eta_0^{-1}, \eta_0)$ with $\eta_0 = 3.139\,278$, and $b(\eta) < 0$ in $\eta \in (0, \eta_0^{-1}) \cup (\eta_0, \infty)$. At exactly $\eta = \eta_0$ and η_0^{-1} the function $b(\eta)$ vanishes†, so at these points the leading term in (41) vanishes and its behaviour is controlled by the subleading term. In this model it can be written as

$$\left.\frac{J_l(CV)}{J_c^{\text{torus}}}\right|_{\eta=\eta_0} = 1 - \frac{c \log l}{l^2} + \cdots. \tag{42}$$

The behaviour of $b(\eta)$ as a function of the shape of the torus is explained as a highly non-trivial interplay between the different terms which appear in the expression of the partition function. We believe that the same feature is present in the Ising model on the truncated tetrahedron. In this case, the shape of the lattice is fixed, but the chosen boundary conditions are the basic ingredient which makes the leading term in (41) vanish. We do not understand why, apparently, the next-to-leading term of the model considered here is not of the form given by (42). Furthermore, we tried to fit our data to equation (42) and we found a worse χ^2 value than the one presented in section 3.2. For instance, using the last four points ($N \geqslant 9$) we obtained $\chi^2 = 8.8$ with three degrees of freedom. However, it would be interesting to study larger lattices in order to verify our conclusions concerning that point.

We should mention that our conclusions may not apply to the antiferromagnetic regime. The reason is that for such boundary conditions, the lattice is not bipartite. Thus, the phenomenon of frustration may occur in that regime. This feature is absent in the Ising model on the torus. In this case, the lattice is bipartite and for sufficiently low temperatures we find a Néel ground state. This question, on the tetrahedron, is currently under research.

Finally, we would like to say a few words about the continuum theory which is attained in the thermodynamic limit. The evidence we have found for scaling suggests a description in terms of the fields and weights of a conformal field theory. This cannot be a trivial example of field theory on the sphere (or on the plane), since four curvature singularities arise which cannot be removed by conformal transformations. Under the assumption of conformal invariance, though, we could still stick three of the vertices together (at a point we may take as infinity) by means of $SL(2, C)$ transformations, leaving a lone singularity in the bulk. This picture is close in spirit to the Coulomb gas representation of conformal field theories but with the difference that now not all the curvature is pinched at the point at infinity. A conical singularity on the plane may have sensible effects on the correlation functions of the theory. We recall here another example with non-trivial boundary conditions, namely

† The same occurs for $\eta = 0, \infty$ [5].

that of a conformal field theory on the semiplane. In this case, correlators which are taken at a finite distance to the boundary do not measure the conformal weights of the theory on the plane [20]. In our model, it may not be necessary to compute correlators that are infinitely far away from the singularity to measure bulk conformal weights, but again some dependence on the location of the points should be expected. This point deserves further clarification, though its investigation in the lattice would require more powerful computer facilities than those used in the present work.

Acknowledgments

We thank Juan Jesús Ruiz-Lorenzo and Miguel Angel Martín-Delgado for helpful discussions. We acknowledge the financial support of the CICyT.

References

[1] Onsager L 1944 *Phys. Rev.* **65** 117
[2] Kasteleyn P W 1963 *J. Math. Phys.* 4 287
[3] Houtappel R M F 1950 *Physica* **16** 425
Husimi K and Syozi I 1950 *Prog. Theor. Phys.* **5** 177
Wannier G H 1950 *Phys. Rev.* **79** 357
Stephenson J 1964 *J. Math. Phys.* **5** 1009
[4] Barber M N 1983 Finite-size scaling *Phase Transitions and Critical Phenomena* vol 8, ed C Domb and J L Lebowitz (New York: Academic)
[5] Ferdinand A E and Fisher M E 1969 *Phys. Rev.* **185** 832
[6] Fisher M E 1971 *Critical Phenomena (Proc. Enrico Fermi Summer School)* ed M S Green (New York: Academic)
Fisher M E and Barber M N 1972 *Phys. Rev. Lett.* **28** 1516
[7] González J and Martín-Delgado M A 1993 Exact finite-size results on the Ising model in 2D curved space *Preprint* PUPT-1367 (bulletin board hep-th/9301057)
[8] Cardy J L 1987 *Nucl. Phys.* B **229** 355
Cardy J L and Peschel I 1988 *Nucl. Phys.* B **300** 377
Cardy J L and Lewellen D C 1991 *Phys. Lett.* **259B** 274
Cardy J L 1984 *J. Phys. A: Math. Gen.* **17** L385
[9] Polyakov D 1992 Curvature singularity as the vertex operator *Preprint* Rutgers RU-92-63 (bulletin board hep-th/9302017)
[10] Montroll E W 1968 *Lectures on the Ising Model of Phase Transitions (Brandeis University Summer Institute in Theoretical Physics, 1966)* ed M Chrétien *et al* (New York: Gordon and Breach)
[11] McCoy B M and Wu T T 1973 *The Two-Dimensional Ising Model* (Cambridge, MA: Harvard University Press)
[12] Fisher M E and Barber M N 1973 *Ann. Phys.* **77** 10
Barber M N 1973 *Aust. J. Phys.* **26** 483
[13] Asorey M, Esteve J G and Salas J 1993 Finite size analysis of the one-dimensional $q = \infty$ clock model *Preprint* DFTUZ 93.3. (bulletin board hep-lat/9305022)
[14] Itzykson C and Drouffe J-M 1989 *Statistical Field Theory* vol 1 (Cambridge: Cambridge University Press)
[15] Baxter R J 1990 *Exactly Soluble Models in Statistical Mechanics* (New York: Academic)
[16] Ferremberg A M, Landau D P and Wong Y J 1992 *Phys. Rev. Lett.* **69** 3382
Vattulainen I, Kankaala K, Saarinen J and Ala-Nissila T 1993 A comparative study of some pseudorandom number generators *Preprint* HU–TFT–93–22 (bulletin board hep-lat/9304008)
[17] Sokal A D 1989 *Monte Carlo Methods in Statistical Mechanics: Foundations and New Algorithms (Cours de la Troisième Cycle de la Physique en Suisse Romande, Lausanne, 1989)*
Wolff U 1989 *Phys. Lett.* **228B** 379
[18] Falcioni M *et al* 1982 *Phys. Lett.* **108B** 331
Ferrenberg A M and Swendsen R H 1988 *Phys. Rev. Lett.* **61** 2635; 1989 *Phys. Rev. Lett.* **63** 1195
[19] Fukugita M, Okawa M and Ukawa A 1990 *Nucl. Phys.* B **337** 181
[20] Cardy J L 1984 *Nucl. Phys.* B **240** 514